Z. Phys. B – Condensed Matter 41, 251–258 (1981)

Condensed Matter
Zeitschrift für Physik B

Nonlinear Renormalization-Group Analysis Applied to the Hydrodynamic Light Scattering Spectrum of ^{4}He below T_λ

V. Dohm
Institut für Festkörperforschung der Kernforschungsanlage Jülich, Federal Republic of Germany

R. Folk*
Institut für Theoretische Physik, Universität Linz, Austria**
und Institut für Festkörperforschung, Kernforschungsanlage Jülich, Federal Republic of Germany

Received November 21, 1980

We calculate the observable critical temperature dependence of the transport coefficients entering the hydrodynamic form of the dynamic structure factor of ^{4}He below T_λ. Application of our recently introduced nonlinear renormalization-group analysis yields quantitative agreement with previous light scattering experiments in the hydrodynamic region. This resolves a long-standing problem in the critical dynamics below the superfluid transition of ^{4}He.

I. Introduction

Progress has been achieved recently in the understanding of the asymptotic and nonasymptotic critical dynamics of the superfluid transition in ^{4}He [1–15]. On the basis of a linearized treatment of the departures from the asymptotic critical dynamics, improved agreement was found between theory and thermal conductivity and light scattering data above T_λ [7–10]. Subsequently it was shown [13, 15] that such departures can be properly accounted for only by means of a fully nonlinear (rather than linear [1, 7] or quadratic [14]) renormalization-group analysis. The effective ratio $w(l)$ of the relaxation rates of the order parameter and the entropy and the effective dynamic coupling $f(l)$ were found to exhibit a nontrivial dependence on the flow parameter l in the experimentally accessible regime which causes large, temperature dependent departures from the asymptotic universal [16–18, 12] ratios R_λ and R_2 entering thermal conductivity and second-sound damping. This led to the quantitative explanation of thermal conductivity data [19–22] over several decades in relative temperature and of second-sound damping measurements [23, 24] at saturated vapor pressure [13, 15]. More recently, also light scattering experiments (at higher pressure) [25] in the hydrodynamic region above and below T_λ were explained by means of our nonlinear analysis [15].

In the present paper we extend the nonlinear treatment to the complete second-sound part of the dynamic structure factor in the hydrodynamic region below T_λ. On the basis of a oneloop calculation of the corresponding transport coefficients we shall find that the nonlinear analysis accounts well for the light scattering data of Winterling, Holmes and Greytak [26], of Tarvin, Vidal and Greytak [25], and of Vinen and Hurd [27] and thus resolves a long-standing problem of the critical dynamics in the hydrodynamic region of the superfluid transition of ^{4}He [28].

II. Nonasymptotic Critical Temperature Dependence of the Dynamic Structure Factor

It is well known that the dynamic structure factor $S(k, \omega)$ near T_λ can be approximated by two separate

* Supported in part by the Fonds zur Förderung der wissenschaftlichen Forschung
** Permanent address

0340-224X/81/0041/0251/$01.60

contributions $S_1(k,\omega)$ and $S_2(k,\omega)$ due to first- and second-sound [29]. In the hydrodynamic region below T_λ, $S_2(k,\omega)$ has the form [29]

$$S_2(k,\omega)=\text{const.}\frac{D_\kappa\,\omega^2 k^2+D_\zeta c_2^2 k^4}{(c_2^2 k^2-\omega^2)^2+D_2^2\,\omega^2 k^4}, \tag{1}$$

$$D_2=D_\zeta+D_\kappa, \tag{2}$$

where c_2 and D_2 are the velocity and damping of second-sound, respectively.

Dynamic scaling theory predicted [30] the damping D_2 to increase near T_λ as

$$D_2\sim(T_\lambda-T)^{-1/3}, \tag{3}$$

in good agreement with subsequent second-sound damping measurements at low frequencies [31] but in disagreement with light scattering experiments [25-27]. The latter exhibited only a weak temperature dependence of the halfwidth

$$\Gamma_2=\tfrac{1}{2}D_2 k^2 \tag{4}$$

whose magnitude, in the hydrodynamic region, was much higher than that obtained from mode-coupling calculations [18]. Also the ratio D_ζ/D_κ was measured near T_λ [25-27] and was found to be of the order of 2, in contrast to the prediction $D_\zeta/D_\kappa=0.36$ of the symmetric planar-spin model (model E) [18] quoted by Tarvin et al. [25], by Vinen and Hurd [27], and by Greytak [32].

Recently we showed that our nonlinear renormalizationgroup analysis accounts well for both the magnitude and temperature dependence of the halfwidth Γ_2 [15]. So far, to our knowledge, no calculation is available in the literature for the separate contributions D_ζ and D_κ near T_λ. In this Section we shall present the result of a corresponding calculation in lowest nontrivial order of the static and dynamic couplings.

The entropy correlation function calculated within model F [16], or, approximately, within model E [16-18] should provide the appropriate description for the dynamic structure factor (1). We have performed a field-theoretic one-loop calculation to obtain the nonasymptotic critical temperature dependence of D_ζ and D_κ. The computational part is identical with that outlined recently [12] for the asymptotic scaling region. The analytic expressions for D_κ and D_ζ within model E read in one-loop order

$$D_\kappa=\chi_0^{-1}\,\lambda(l)\left\{1-\frac{f(l)}{4}\ln\frac{-2\tau(l)}{\mu^2 l^2}\right.$$
$$\left.+f(l)\,F_\kappa[w(l),f(l)]\right\}, \tag{5}$$

$$D_\zeta=\chi_0^{-1}\,\lambda(l)\,w(l)\left\{1-\frac{f(l)}{2(1+w(l))}\ln\frac{-2\tau(l)}{\mu^2 l^2}\right.$$
$$\left.+f(l)\,F_\zeta[w(l),f(l)]+u^*\,U_\zeta[w(l),f(l)]\right\}, \tag{6}$$

with

$$\lambda(l)=\left(\frac{K_d\,g_0^2\,\chi_0}{(\mu\,l)^\varepsilon\,w(l)\,f(l)}\right)^{1/2}, \tag{7}$$

where $K_d^{-1}=2^{d-1}\,\pi^{d/2}\,\Gamma(d/2)$, $u^*=\varepsilon/40$, $d=4-\varepsilon$. The functions F_κ, F_ζ and U_ζ are given in the Appendix. In (5)-(7) we have employed our previous notation [15]; thus the effective ratio of relaxation rates $w(l)$ and the effective dynamic coupling $f(l)$ satisfy the flow equations

$$l\frac{dw(l)}{dl}=\beta_w[w(l),f(l)], \tag{8}$$

$$l\frac{df(l)}{dl}=\beta_f[w(l),f(l)], \tag{9}$$

with nonuniversal initial conditions $w(1)$, $f(1)$ and asymptotic fixed point values $w^*=w(0), f^*=f(0)$. For β_w and β_f we use the two-loop results of De Dominicis and Peliti [1] and of one of the present authors [3]. For simplicity we neglect static corrections to scaling.

The effective temperature variable $\tau(l)$ is given by

$$\tau(l)=\tau(1)\exp\int_1^l \zeta_\tau\frac{dl'}{l'}, \tag{10}$$

$$\tau(1)=a\frac{T-T_\lambda}{T_\lambda}\equiv a\,t,\qquad a>0, \tag{11}$$

where ζ_τ is determined by the static Z-factor renormalizing the bare temperature variable τ_0 [15]. Apart from static corrections to scaling we have

$$\tau(l)=t\,\mu^2\,l^2\,l^{-1/\nu}A^{-1}, \tag{12}$$

$$A=a^{-1}\,\mu^2\exp\int_0^1(\zeta_\tau-\zeta_\tau^*)\frac{dl'}{l'}, \tag{13}$$

with $\nu=(2-\zeta_\tau^*)^{-1}$. Since the constants A and μ are independent of whether $T>T_\lambda$ or $T<T_\lambda$ we employ our previous choice [15]

$$A=1,\qquad \mu=\xi_0^{-1}, \tag{14}$$

where ξ_0 appears in the correlation length

$$\xi_+=\xi_0\,t^{-\nu} \tag{15}$$

above T_λ.

We choose the connection between the relative temperature $-t>0$ below T_λ and the flow parameter

$l>0$ in the usual way [33]

$$\frac{-2\tau(l)}{\mu^2 l^2}=1 \tag{16}$$

in which case the logarithms in (5) and (6) drop out. Equations (12), (14), and (16) imply

$$l=(-2t)^\nu, \qquad T<T_\lambda. \tag{17}$$

From (2), (5), (6), and (16) we obtain

$$D_2=\chi_0^{-1}\,\lambda(l)\,\Phi[w(l),f(l)] \tag{18}$$

with the function [13]

$$\Phi[w,f]=1+w+u^*\,w\,U_\zeta+f(F_\kappa+w\,F_\zeta). \tag{19}$$

The remaining task is to identify the nonuniversal initial conditions $w(1)$, $f(1)$ and to perform an appropriate comparison with light scattering experiments.

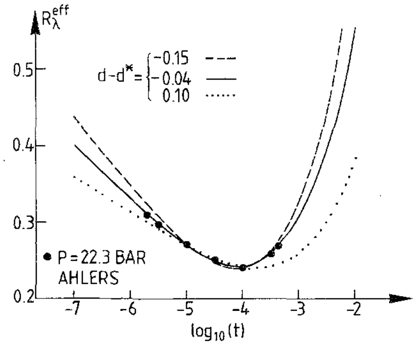

Fig. 1. Experimental values (heavy dots) for $R_\lambda^{\exp}$ according to (21) at the pressure of 22.3 bar extracted from Ahlers' measurements [20, 34, 35]. Only representative values are shown. The curves are two-parameter fits of R_λ^{eff}, (20), at different fixed deviations $d-d^*$ of the model dimension d from the two-loop estimate for the borderline dimension d^* where dynamic scaling breaks down. The full curve corresponds to the initial conditions $w(l_0)=0.70, f(l_0)=0.57$ at $l_0=10^{-2}$ ($t_0=l_0^{1/\nu}=10^{-3}$). The present analysis suggests $|3-d^*|\lesssim 0.1$ (provided that the presently available data represent the true critical behavior)

III. Comparison with Experiments

A. Determination of the Nonuniversal Initial Conditions

As we are interested in a comparison with light scattering experiments at higher pressures [25–27, 32] we use Ahlers' thermal conductivity data at 22.3 bar above T_λ [20, 34, 35] in order to determine $w(1)$ and $f(1)$. The procedure is that introduced previously [13]. Thus we fit the effective ratio

$$R_\lambda^{\mathrm{eff}}=\left(\frac{K_3}{w(l)f(l)}\right)^{1/2}\left(1-\frac{f(l)}{4}\right) \tag{20}$$

(with $l=t^{2/3}$) to its experimental counterpart

$$R_\lambda^{\exp}(t)=\frac{\lambda(t)}{g_0\,\xi_+^{1/2}\,k_B^{1/2}\,C_p(t)^{1/2}} \tag{21}$$

where $\lambda(t)$ and $C_p(t)$ are Ahlers' experimental values for the thermal conductivity [20, 34, 35] and specific heat [36] at 22.3 bar, in units of erg $\mathrm{K}^{-1}\,\mathrm{s}^{-1}\,\mathrm{cm}^{-1}$ and erg $\mathrm{K}^{-1}\,\mathrm{cm}^{-3}$, respectively. For $g_0=k_B TS/R\hbar$ we find, from measurements [36] of the entropy $S=4.88$ J/mol K at 22.3 bar, $g_0=1.45\cdot 10^{11}\,s^{-1}$ for $T=T_\lambda=1.89$ K. For ξ_+ we take $\xi_+=\xi_0 t^{-2/3}$, $\xi_0=1.41\cdot 10^{-8}$ cm [37].
Representative values for $R_\lambda^{\exp}(t)$ are shown in Fig. 1. As previously at saturated vapor pressure, an excellent fit was possible for $d-d^*=-0.04$ where $d^*\approx 3$ is a two-loop estimate for the borderline dimension below which dynamic scaling breaks down (the fit quality is independent of the precise value of d^*). As seen from the dashed and dotted curves in Fig. 1, the presently available data appear to indicate $|d^*-3|\lesssim 0(0.1)$. [We recall that this conclusion is, of course, based on the interpretation that Ahlers' data [20, 34, 35] represent the true critical behavior of the thermal conductivity of ^{4}He, and that model E is sufficiently accurate, see the reservations made in [15].] The fit corresponding to the full curve in Fig. 1 yields the initial conditions, for example at $l=10^{-2}$, $w(10^{-2})=0.70$, $f(10^{-2})=0.57$, as noted recently [15], or

$$w(1)=0.81, \qquad f(1)=0.01. \tag{22}$$

The corresponding $w(l)$ and $f(l)$ are shown in Figs. 2a and b which are similar to the full curves in Figs. 7a and b of the previous case [15] at saturated vapor pressure. Again the minimum of R_λ^{eff} (Fig. 1) near $t=10^{-4}$ ($l=10^{-8/3}$) is the result of a competition between *an increasing $w(l)$ and a decreasing $f(l)$ as l increases.*

B. Comparison of D_κ with Experiment

As is well known [16] the slow approach of the specific heat to its finite value at T_λ induces effects that are not contained in model E. They can be included with reasonable accuracy, however, by replacing χ_0 by the *experimental* constant-pressure specific heat per unit volume C_p divided by k_B [16]. From (5), (7), (16), and (17) we then obtain in $d=3$ dimensions

$$D_\kappa(-t)=\left(\frac{g_0^2\,k_B\,\xi_0(-2t)^{-2/3}}{2\pi^2\,C_p^-(-t)\,w(l)f(l)}\right)^{1/2}\cdot\{1+f(l)\,F_\kappa[w(l),f(l)]\} \tag{23}$$

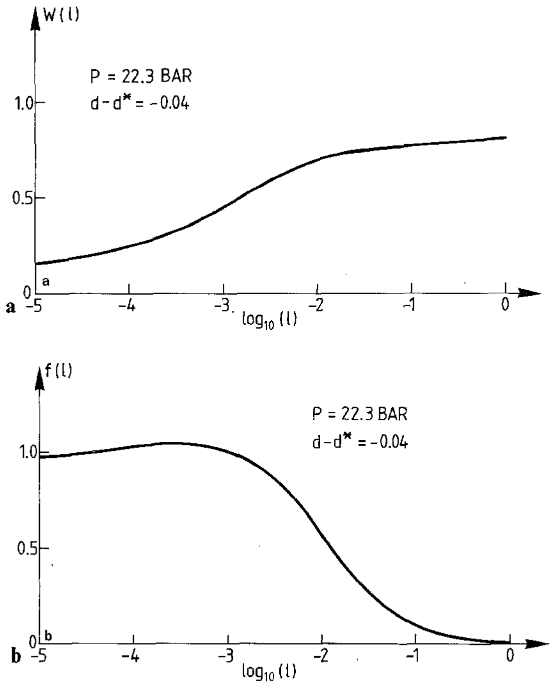

Fig. 2a, b. Effective ratio of relaxation rates $w(l)$ and effective dynamic coupling $f(l)$ versus flow parameter l from (2.13)–(2.17), (A3) –(A6) of [15], with initial conditions adjusted such that R_λ^{eff}, (20), fits R_λ^{exp}, (21), at 22.3 bar. The corresponding fit is shown in Fig. 1 (full curve, $d-d^*=-0.04$). The parameters $w(l)$ and $f(l)$ identify a particular trajectory in the flow diagram of Fig. 1b of [15] corresponding to ^{4}He at 22.3 bar

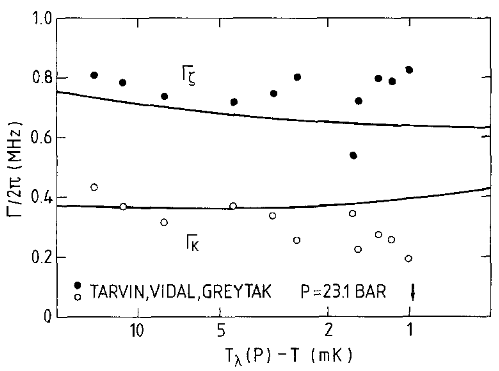

Fig. 3. Experimental data for the two separate contributions $\Gamma_\zeta=\frac{1}{2}D_\zeta k^2$ and $\Gamma_\kappa=\frac{1}{2}D_\kappa k^2$ to the hydrodynamic linewidth at a pressure of 23.1 bars, $k=1.79\cdot 10^5\,\mathrm{cm}^{-1}$, taken from Fig. 10 of [25]. Full curves from (23) and (31)–(34), with $w(l)$ and $f(l)$ according to Fig. 2, $l=(-2t)^{2/3}$. The arrow indicates where $k\xi_T=1$

where C_p^- is the experimental specific heat at 22.3 bar below T_λ [36].

Equation (23) is our final result for D_κ. The direct comparison with light scattering experiment (at 23.1 bar) [25] is shown in Fig. 3 (lower curve). Excellent agreement is found in the hydrodynamic region up to $k\xi_T\sim 0.5$. The temperature regime shown in Fig. 3 corresponds to $10^{-2}\lesssim l\lesssim 10^{-1}$ where $f(l)$ decreases significantly whereas $w(l)$ increases slowly, according to Fig. 2.

C. Comparison of D_2 with Experiment

Our procedure will be to first determine the effective ratio

$$R_2^{\mathrm{eff}}=\frac{D_2}{2c_2\xi_T} \tag{24}$$

within model E and then to include the specific heat effect in D_2 via experimental values c_2^{exp} for the second-sound velocity [13, 15]. In (24) ξ_T is the transverse correlation length [38]. Within model E the second-sound velocity is given by [17]

$$c_2=\chi_0^{-1/2}g_0\bar{\psi}\bar{\chi}_T^{-1/2}, \tag{25}$$

$$\bar{\chi}_T=1-2u^*+O(u^{*2}), \tag{26}$$

where $\bar{\psi}$ is the spontaneous value of the order parameter. Using (7), (18), (24), and (25) we obtain

$$R_2^{\mathrm{eff}}=\left(\frac{2u^*\bar{\chi}_T\xi_L^{d-2}}{(\mu l)^\varepsilon\xi_T^2\,w(l)f(l)}\right)^{1/2}\Phi[w(l),f(l)] \tag{27}$$

where $\Phi[w,f]$ is given by (19) and ξ_L is defined by

$$\xi_L^{-2\beta/\nu}=\xi_L^{2-d-\eta}\equiv 8u^*\bar{\psi}^2K_d^{-1} \tag{28}$$

Inserting $\mu_0=\xi_0^{-1}$ and $l=(-2t)^\nu$ according to (14) and (17) yields in $d=3$ dimensions*

$$R_2^{\mathrm{eff}}(-t)=\left(\frac{\xi_L\xi_0(-2t)^{-2/3}}{\xi_T^2}\right)^{1/2}\left(\frac{2u^*(1-2u^*)}{w(l)f(l)}\right)^{1/2}\Phi[w(l),f(l)] \tag{29}$$

with $\xi_T=\xi_-(-t)^{-2/3}$ where [37]

$$\xi_-=3.57\cdot 10^{-8}\,\mathrm{cm}. \tag{30}$$

For ξ_L/ξ_T we take 0.33 [18]. In Fig. 4 R_2^{eff} is shown for 22.3 bar according to the fit of R_λ^{eff} to the thermal conductivity data above T_λ. The temperature dependence of R_2^{eff} for $10^{-6}\lesssim|t|\lesssim 10^{-4}$ is weaker than that in case of R_λ^{eff} since $R_2^{\mathrm{eff}}\sim(wf)^{-1/2}(1+w)$ is less sensitive to the variation of w than $R_\lambda^{\mathrm{eff}}\sim(wf)^{-1/2}$ in this regime. The strong increase of both R_2^{eff} and R_λ^{eff} for $t\gtrsim 10^{-3}$ is due to the decreasing f for $l\gtrsim 10^{-2}$.

For the purpose of a comparison with experiment we employ the experimental values c_2^{exp} for the second-sound velocity [34]. This yields the damping

$$D_2=2c_2^{\mathrm{exp}}\xi_TR_2^{\mathrm{eff}} \tag{31}$$

* An alternative way of treating the static part of the prefactor in (27) is to set $\mu^2l^2=-2\tau(l)=8(\mu l)^\varepsilon\,u^*\bar{\psi}^2K_d^{-1}$, hence $\mu l=\xi_L^{-1}$ which corresponds to Siggia's treatment [17]. This yields R_2^{eff} in the previous form [13]. Both types of treatment will be compared in more detail elsewhere. The slight difference between the full curves of Fig. 8 in [15] and in Fig. 5 below is due to these different treatments

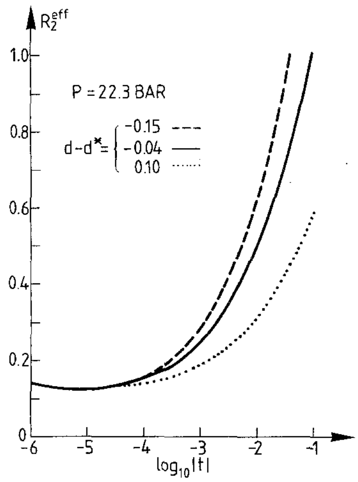

Fig. 4. Effective theoretical amplitude ratio $R_2^{\rm eff}$, (29), entering second-sound damping at 22.3 bar corresponding to the fits of $R_\lambda^{\rm eff}$ in Fig. 1

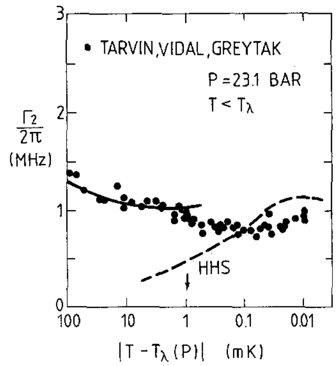

Fig. 5. Halfwidth for the dynamic structure factor measured by Tarvin et al. [25]. The dashed curve represents the result of [18], the solid curve represents (32), with $R_2^{\rm eff}$ from (29) corresponding to the full curve in Fig. 4. The arrow indicates where $k\xi_T=1$. The present theory is applicable only to the hydrodynamic region $k\xi_T<1$. For $T>T_\lambda$ see Fig. 8 of [15]

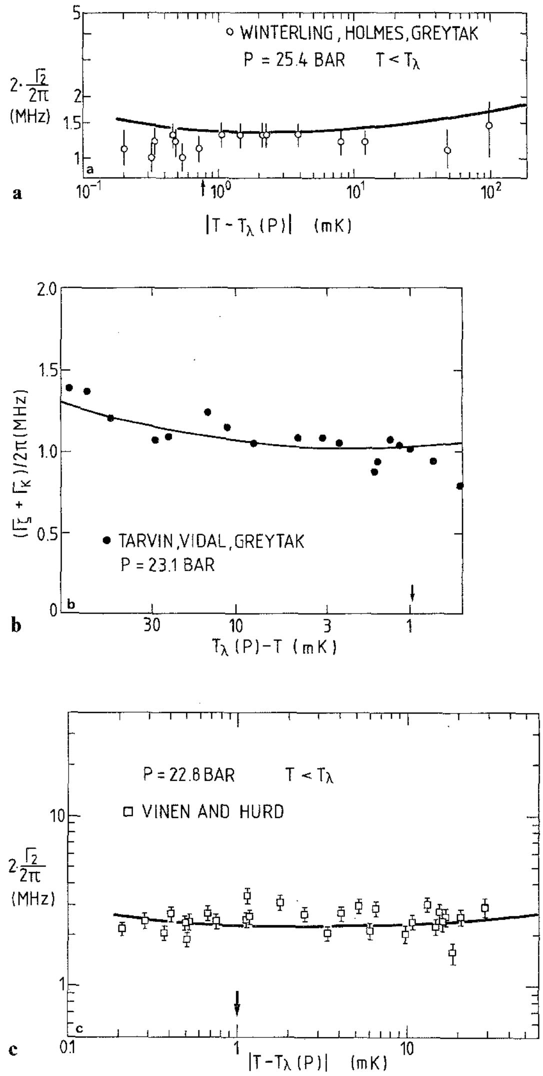

Fig. 6a–c. Light scattering data for the halfwidth Γ_2 of the hydrodynamic second-sound spectrum: (**a**): at 25.4 bar, $k=1.45\cdot 10^5\,{\rm cm}^{-1}$ [26], (**b**): at 23.1 bar, $k=1.79\cdot 10^5\,{\rm cm}^{-1}$ [25], (**c**): at 22.8 bar, $k=1.88\cdot 10^5\,{\rm cm}^{-1}$ [27]. Full curves from (32) with $R_2^{\rm eff}$ from (29) corresponding to the full curve in Fig. 4. The arrows indicate where $k\xi_T=1$. The full curve in (**b**) is also show in Fig. 5

and the halfwidth

$$\Gamma_2=c_2^{\rm exp}\,\xi_T R_2^{\rm eff}k^2 \qquad (32)$$

with $R_2^{\rm eff}$ given by (29).

A comparison of D_2 with low-frequency measurements was already presented recently [13]. Here we turn to the light scattering data [25–27] which could not be explained by asymptotic theories [17, 18] (Fig. 5, dashed curve). Also a recent preliminary attempt [10, 11] to include background effects could not account for the light scattering experiments in the hydrodynamic region below T_λ (see Fig. 7 of [10]).

In Figs. 5 and 6a–c our expression for Γ_2, (32), (29), is compared with three independent light scattering experiments [25–27] at slightly different pressures. Our theory agrees well with these data both in magnitude and in temperature dependence. The latter is weak because the strong decrease of $f(l)$ in the regime $10^{-2}\lesssim l\lesssim 10^{-1}$ essentially compensates the temperature dependence of $c_2^{\rm exp}\,\xi_T$ which should otherwise lead to the predicted $(T_\lambda-T)^{-1/3}$ behavior [30] in the hydrodynamic region (apart from deviations due to the specific heat). A similar effect shows up above T_λ [15].

D. Comparison of D_ζ with Experiment

Within model E (rather than model F) it is not unique how to properly include the specific heat effects

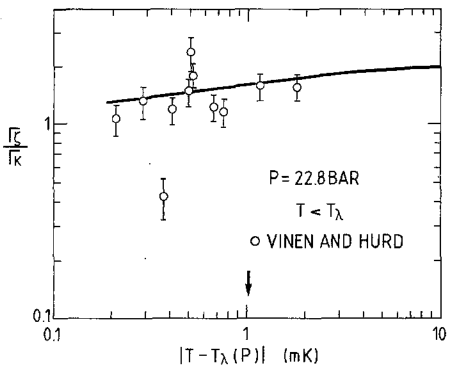

Fig. 7. Ratio of the coefficients Γ_ζ and Γ_κ contributing to the hydrodynamic linewidth of the dynamic structure factor. Circles from Fig. 12 of Vinen and Hurd [27], full curve from (34) and (23)

in the expression (6) for D_ζ directly. Therefore we determine D_ζ via (2),

$$D_\zeta = D_2 - D_\kappa \tag{33}$$

where we use (31) and (23) for D_2 and D_κ, respectively. The resulting

$$\Gamma_\zeta = \tfrac{1}{2} D_\zeta k^2 \tag{34}$$

is compared with experiment [25] in Fig. 3 (upper curve). The agreement is reasonable (within the expected accuracy of model E). A further comparison of D_ζ with experiment [27] is shown in Fig. 7 where the ratio $\Gamma_\zeta/\Gamma_\kappa = D_\zeta/D_\kappa$ is plotted. The agreement is satisfactory.

IV. Summary

We have calculated the critical temperature dependence of hydrodynamic transport coefficients of ^{4}He below T_λ within model E and have applied our recently introduced nonlinear renormalization-group analysis in order to perform a quantitative comparison with light scattering experiments. The nonuniversal parameters have been determined independently from Ahlers' thermal conductivity data at 22.3 bar above T_λ [20, 34, 35]. Satisfactory agreement with the light scattering data (at similar pressures) below T_λ was found for $k\xi_T \lesssim 1$. Thus, together with the recent explanation of thermal conductivity and low-frequency second-sound damping measurements, agreement between theory and experiment in the hydrodynamic region above and below T_λ is established with reasonable accuracy.

In all cases the explanation of the experiments follows naturally from the l-dependence $[l \sim |t|^{2/3}]$ of the effective parameters $w(l)$ and $f(l)$. In particular:

(i) The approximate verification of the scaling prediction for D_2, (3), by Tyson [31] in the regime $-t < 10^{-3}$ is consistent with the weak temperature dependence of R_2^{eff} in this regime [13]; this is due to the fact that $R_2^{\mathrm{eff}} \sim (wf)^{-1/2}(1+w)$ is not very sensitive to a variation of w in this regime ($l < 10^{-2}$), and $f(l)$ is weakly l-dependent for $l < 10^{-2}$ at saturated vapor pressure.

(ii) The hydrodynamic region probed by light scattering experiments at larger k [25–27] corresponds to the regime $10^{-2} \lesssim l \lesssim 10^{-1}$ where $w(l)$ is slowly rising and $f(l)$ is strongly decreasing. This decrease of $f(l)$ implies the increase of $R_2^{\mathrm{eff}} \sim f^{-1/2}$ as l increases and therefore essentially compensates the temperature dependence of $c_2 \xi_T$ in the measured halfwidth $\Gamma_2 = c_2 \xi_T R_2^{\mathrm{eff}} k^2$. A corresponding statement holds above T_λ.

The present theory is limited to the hydrodynamic region because of the approximation $k\xi_T \ll 1$ employed in calculating the entropy correlation function. This is the reason why our expression for Γ_2 corresponding to the full curve in Fig. 5 would diverge if it were formally extrapolated to $k\xi_T \gg 1$. An analytic treatment including the critical region has been performed previously [39] and is presently being compared with experiment [28].

Finally we again point to the main sources of possible inaccuracies of our results:

(1) We have used the flow equations of model E which are known only in the two-loop approximation.

(2) We have employed model E rather than model F for which the complete two-loop results are as yet unknown. This model provides one additional fit parameter [14].

(3) Ahlers' data at 22.3 bar that were available to us [20, 34, 35] may not represent the true critical behavior of the ^{4}He thermal conductivity (see the note below, see also [40]), therefore our identification of nonuniversal parameters via these data may be modified in a future more refined analysis. For the regime $l \gtrsim 10^{-2}$ which is relevant for the light scattering experiments studied in this paper this modification may be negligible.

(4) We have neglected static corrections to scaling.

(5) The static part of the prefactor in (27) is not accurately known.

After the present work was completed we received a preprint by Ahlers, Hohenberg and Kornblit where the authors extend our previous nonlinear analysis of model E [13, 15] to model F (as far as its flow equations are known [1, 16]. They apply this analysis both to previous as well as to new thermal conductivity data at saturated vapor pressure. The new data differ appreciably from the previous ones for $t<10^{-3}$ and suggest the stability of the scaling fixed point in $d=3$ dimensions (provided that the new data represent the true ^{4}He critical thermal conductivity). The authors confirm the decrease of $f(l)$ for $l>10^{-2}$ towards a "weak-coupling regime", which was originally found earlier in [13, 15], see in particular Figs. 1, 2, 3, 7 of [15].

One of us (V.D.) would like to thank C. De Dominicis for useful discussions.

Appendix

The function $F_\kappa[w,f]$ in (5) reads

$$F_\kappa[w,f]=\tfrac{1}{8}+\tfrac{1}{8}G(w,f)+\tfrac{1}{4}H(w,f) \tag{A1}$$

where

$$G(w,f)=a_1\left[b_-^{(1)}\ln\frac{b_-^{(1)}}{4(1+w)} - b_+^{(1)}\ln\frac{b_+^{(1)}}{4(1+w)}\right] \tag{A2}$$

and

$$H(w,f)=(x-2)^{-1}\{(w+x)\,a_2\ln[b_-^{(2)}/b_+^{(2)}] + \ln[2(1+w)/w]\} \tag{A3}$$

with

$$x=1+\frac{f}{8u}, \tag{A4}$$

$$a_1=(5w^2+6xw+x^2)^{-1/2}, \tag{A5}$$

$$a_2=(w^2+6xw-8w+x^2)^{-1/2}, \tag{A6}$$

$$b_\pm^{(1)}=3w+x\pm a_1^{-1}, \tag{A7}$$

$$b_\pm^{(2)}=3w+x\pm a_2^{-1}. \tag{A8}$$

The term 1/8 in (A1) corrects our previous expressions for $F_f(w)$ in (13) of [12] and for $\phi[w,f]$ in (11) of [13] where a corresponding term should be added.

The functions $U_\zeta[w,f]$ and $F_\zeta[w,f]$ in (6) are given by

$$U_\zeta[w,f]=2+2(x-2)^{-1}\{(3w-x-2wx)\,a_2 \ln[b_+^{(2)}/b_-^{(2)}]+\ln[2(1+w)/w]\}, \tag{A9}$$

$$F_\zeta[w,f]=\tfrac{3}{4}H[w,f]+\frac{G[w,f]}{4(1+w)}. \tag{A10}$$

In the one-loop calculation the term $f/8u$ in x, (A4), arises from

$$\frac{g_0^2}{\lambda(l)\Gamma(l)}\frac{\bar{\psi}^2}{\mu^2 l^2}=K_d^{-1}f(l)(\mu l)^\varepsilon\bar{\psi}^2/(\mu l)^2 \tag{A11}$$

$$=\frac{f(l)}{8u(l)}. \tag{A12}$$

In the comparison with experiment in Sect. III we have used in (A11)

$$\mu=\xi_0^{-1},\qquad l=(-2t)^\nu, \tag{A13}$$

$$\bar{\psi}^2=c_2^2\chi_0 g_0^{-2}[1+O(u)], \tag{A14}$$

[see (14), (17), (25)] and have employed experimental values for c_2 and χ_0. Thus we have evaluated x according to

$$x=1+f(l)\cdot\frac{2\pi^2\xi_0 C_p^-(c_2^{\exp})^2}{g_0^2 k_B(-2t)^{2/3}}. \tag{A15}$$

References

1. Dominicis, C. De, Peliti, L.: Phys. Rev. Lett. **38**, 505 (1977); Phys. Rev. B **18**, 353 (1978)
2. Dohm, V., Ferrell, R.A.: Phys. Lett. **67A**, 387 (1978)
3. Dohm, V.: Z. Phys. B - Condensed Matter **31**, 327 (1978)
4. Ferrell, R.A., Dohm, V., Bhattacharjee, J.K.: Phys. Rev. Lett. **41**, 1818 (1978)
5. Ferrell, R.A., Bhattacharjee, J.K.: J. Low Temp. Phys. **36**, 165 (1979)
6. Dohm, V.: Z. Phys. B - Condensed Matter **33**, 79 (1979)
7. Ferrell, R.A., Bhattacharjee, J.K.: Phys. Rev. Lett. **42**, 1638 (1979)
8. Ferrell, R.A., Bhattacharjee, J.K.: Phys. Rev. **B 20**, 3690 (1979)
9. Ferrell, R.A., Bhattacharjee, J.K.: In: Proceedings of the International Conference on Dynamic Critical Phenomena. Enz, C.P. (ed.). Berlin, Heidelberg, New York: Springer 1979
10. Ferrell, R.A., Bhattacharjee, J.K.: In: Light Scattering in Solids. Birman, J.L., Cummins, H.Z., Rebane, K.K. (eds.), New York: Plenum Press 1979
11. Bhattacharjee, J.K.: Thesis, University of Maryland (1979)
12. Dohm, V., Folk, R.: Z. Phys. B - Condensed Matter **35**, 277 (1979); Z. Phys. B - Condensed Matter **39**, 94 (1980)
13. Dohm, V., Folk, R.: Phys. Rev. Lett. **46**, 349 (1981)
14. Hohenberg, P.C., Halperin, B.I., Nelson, D.R.: Phys. Rev. **B 22**, 2373 (1980)
15. Dohm, V., Folk, R.: Z. Phys. B - Condensed Matter **40**, 79 (1980)
16. Halperin, B.I., Hohenberg, P.C., Siggia, E.D.: Phys. Rev. **B13**, 1299 (1976); **B21** (E), 2044 (1980)
17. Siggia, E.D.: Phys. Rev. **B13**, 3218 (1976)
18. Hohenberg, P.C., Siggia, E.D., Halperin, B.I.: Phys. Rev. **B 14**, 2865 (1976)
19. Ahlers, G.: Phys. Rev. Lett. **21**, 1159 (1968)
20. Ahlers, G.: In: Proceedings of the Twelfth International Conference on Low Temperature Physics. Kanda, E. (ed.), p. 21. Tokyo: Academic Press 1971
21. Kerrisk, J.F., Keller, W.E.: Phys. Rev. **177**, 341 (1969)
22. Bowers, R.: Proc. Phys. Soc. (London), Sect. **A 65**, 511 (1952)

23. Ahlers, G.: Phys. Rev. Lett. **43**, 1417 (1979)
24. Hanson, W.B., Pellam, J.R.: Phys. Rev. **95**, 321 (1954)
25. Tarvin, J.A., Vidal, F., Greytak, T.J.: Phys. Rev. **B 15**, 4193 (1977)
26. Winterling, G., Holmes, F.S., Greytak, T.J.: Phys. Rev. Lett. **30**, 427 (1973)
27. Vinen, W.F., Hurd, D.L.: Adv. Phys. **27**, 533 (1978); Vinen, W.F., Palin, C.J., Lumley, J.M., Hurd, D.L., Vaughan, J.M.: Low Temperature Physics, LT-14. Krusius, M., Vuorio, M. (eds.), Vol. I, p. 191. Amsterdam: North-Holland 1975
28. For a treatment including the more complicated critical region below T_λ see: Dominicis, C. De, Dohm, V.: (in preparation)
29. See e.g. Stephen, M.J.: In: The physics of liquid and solid helium. Bennemann, K.H., Ketterson, J.B. (eds.), Vol. I, Chap. 4. New York: Wiley 1976
30. Ferrell, R.A., Menyhard, N., Schmidt, H., Schwabl, F., Szépfalusy, P.: Phys. Rev. Lett. **18**, 891 (1967); Ann. Phys. (NY) **47**, 565 (1968)
31. Tyson, J.A.: Phys. Rev. Lett. **21**, 1235 (1968)
32. Greytak, T.J.: In: Proceedings of the International Conference on Dynamic Critical Phenomena. Enz, C.P. (ed.). Berlin, Heidelberg, New York: Springer 1979
33. Rudnick, J., Nelson, D.R.: Phys. Rev. **B 13**, 2208 (1976)
34. Ahlers, G.: In: The physics of liquid and solid helium. Bennemann, K.H., Ketterson, J.B. (eds.), Vol. I, Chap. 2. New York: Wiley 1976
35. Ahlers, G.: Rev. Mod. Phys. **52**, 489 (1980)
36. Ahlers, G.: Phys. Rev. **A 8**, 530 (1973)
37. Hohenberg, P.C., Aharony, A., Halperin, B.I., Siggia, E.D.: Phys. Rev. **B 13**, 2986 (1976)
38. See e.g. Hohenberg, P.C., Halperin, B.I.: Rev. Mod. Phys. **49**, 435 (1977)
39. De Dominicis, C., Dohm, V.: unpublished (1979)
40. Archibald, M., Mochel, J.M., Weaver, L.: Phys. Rev. Lett. **21**, 1165 (1968)

V. Dohm
Institut für Festkörperforschung
Kernforschungsanlage Jülich GmbH
Postfach 1913
D-5170 Jülich 1
Federal Republic of Germany

R. Folk
Institut für Theoretische Physik
Universität Linz
A-4045 Linz
Austria

Note Added in Proof

For completeness we compare the results of our theory also with the light scattering data of Winterling, Miller and Greytak [Phys. Lett. **48A**, 343 (1974)] at $p=1.94$ bar below T_λ (Fig. 8) and of Vinen and Hurd [27] at 22.8 bar above T_λ (Fig. 9). The curve in Fig. 8 represents $\Gamma_2/\pi = c_2^{\exp}\,\xi_T\,R_2^{\rm eff}\,k^2/\pi$ with $R_2^{\rm eff}$ given by (29). The curve in Fig. 9 represents $\Gamma_2/\pi = R_\lambda^{\rm eff}\,g_0\,\xi_+^{1/2}\,k_B^{1/2}\,C_p^{-1/2}\,k^2/\pi$ which (apart from the factor 1/2) is also shown in Fig. 8 ($T>T_\lambda$) of [15]. The nonuniversal initial conditions at $l_0=10^{-2}$, as determined from Ahlers' [34] thermal conductivity data at saturated vapor pressure and at 22.3 bar, are $w(l_0)=0.45$, $f(l_0)=0.87$ for Fig. 8 and $w(l_0)=0.70$, $f(l_0)=0.57$ for Fig. 9, respectively, with $d-d^*=-0.04$ in both cases. The curve in Fig. 8 corresponds to the full curve in Fig. 4 of [13]. As noted by Ferrell and Bhattacharjee (preprint January 1981) the light scattering data in Fig. 8 for $k\xi_T<1$ are somewhat higher than expected from the second-sound damping data of Ahlers [23] and of Hanson and Pellam [24]. The arrows in Figs. 8 and 9 indicate the temperatures at which $k\xi_T=1$ and $k\xi_+=1$, respectively.

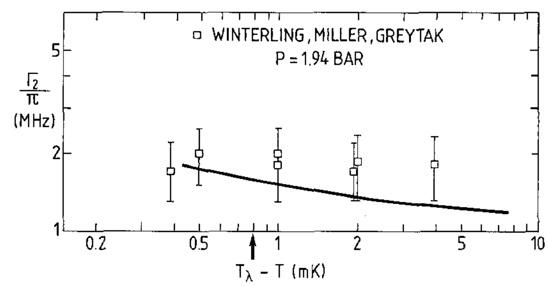

Fig. 8. Halfwidth of the light scattering spectrum as measured by Winterling, Miller and Greytak for $k=1.45\cdot10^5\,\mathrm{cm}^{-1}$ and $P=1.94$ bar. Our theory yields the solid curve

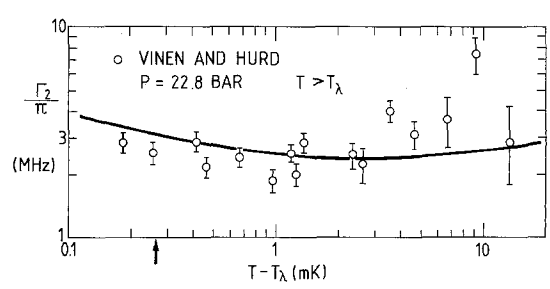

Fig. 9. Halfwidth of the light scattering spectrum as measured by Vinen and Hurd [27] for $k=1.88\cdot10^5\,\mathrm{cm}^{-1}$ and $P=22.8$ bar. Our theory yields the solid curve